AXIAL FEEDBACK STABILIZATION OF FLUTE MODES FOR MIRROR MACHINES

by

B. K. Kang, M. A. Lieberman, and A. K. Sen

Memorandum No. UCB/ERL M86/101

23 December 1986

COVER PAGE

AXIAL FEEDBACK STABILIZATION OF FLUTE MODES FOR MIRROR MACHINES

by

B. K. Kang, M. A. Lieberman, and A. K. Sen

Memorandum No. UCB/ERL M86/101

23 December 1986

ELECTRONICS RESEARCH LABORATORY

College of Engineering
University of California, Berkeley
94720

TITLE PAGE

AXIAL FEEDBACK STABILIZATION OF FLUTE MODES FOR MIRROR MACHINES

by

B. K. Kang, M. A. Lieberman, and A. K. Sen

Memorandum No. UCB/ERL M86/101

23 December 1986

ELECTRONICS RESEARCH LABORATORY

College of Engineering
University of California, Berkeley
94720

AXIAL FEEDBACK STABILIZATION OF FLUTE MODES FOR MIRROR MACHINES

B. K. Kang, M. A. Lieberman, and A. K. Sen[†]

Department of Electrical Engineering and Computer Sciences
and the Electronics Research Laboratory
University of California, Berkeley, CA 94720

Abstract

A novel scheme of feedback stabilization of the $m=1$ flute mode for axisymmetric mirror machines is proposed, which has potential for reactor extrapolation. A three region plasma model is analyzed, consisting of a hot core surrounded by a warm transition annulus, which in turn is surrounded by a warm halo annulus that is in contact with segmented, annular feedback plates at the two endwalls. For plasma parameters characteristics of the TMX-U and MFTF-B devices at The Lawrence Livermore National Laboratory and the MMX device at Berkeley, the required feedback power is calculated. The results show that stability can be achieved in the MMX and TMX-U devices with a modest feedback gain and power. The power requirement for the near-reactor conditions of MFTF-B is more severe, but can be reduced by a modified choice of plasma parameters.

[†]Department of Electrical Engineering, Columbia University, New York, NY 10027

1. Introduction

A promising configuration for fusion plasma confinement is a tandem mirror in which mirror-quadrupole anchor cells are located at the ends of an axisymmetric, central cell solenoid [1,2]. The non-axisymmetric magnetic fields of the anchors form a magnetic well that provides overall magnetohydrodynamic (MHD) stability for curvature-driven flute modes in the plasma, and magnetically confined plasma in the anchors provides axial confinement for center cell ions in the plasma core by maintaining a positive electrostatic potential with respect to the center cell.

To reduce energy loss in the core plasma due to neutral atom penetration, tandem mirrors incorporate an annular, warm plasma layer called a halo plasma. The halo plasma is not axially confined by the electrostatic potentials of the anchors and is lost to the end walls on an MHD flow timescale. Whereas the density of the escaping core plasma near the end walls is very low due to the good axial confinement, the density of the escaping halo plasma near the end walls is of the order of the halo plasma density in the midplane of the device.

Although tandem mirror systems can be economically feasible fusion devices, considerable economic advantage and reduced radial diffusion can be achieved if the anchors are also axisymmetric mirror cells, provided overall stability of the plasma is maintained. The flute mode with azimuthal mode number $m=1$ is the most difficult to stabilize, because it is only weakly influenced by finite larmor radius (FLR) effects that tend to stabilize the higher m modes [3].

Several methods have been proposed to stabilize the $m=1$ flute mode in axisymmetric mirror systems by modifying the admittance of the sheaths that connect the confined plasma to the end walls. One is to increase the admittance of the sheath, thus "line-tying" the plasma to the end wall. However, the sheath provides thermal insulation for the hot core plasma by reducing electron heat conduction to the end wall, and this insulation is degraded severely if the admittance is increased over the entire cross section of the core to achieve stability [4]. Experimentally, stability has been achieved in a low temperature plasma by increasing the admittance using a thermionically emitting endplate [5,6]. Experiments have also been performed using a ring-shaped, emitting endplate that is in contact with only the periphery of the plasma [7-13]. These experiments have demonstrated the stabilizing effect of "surface

line-tying." However, radial temperature gradients can lead to unacceptable heat loss to the halo plasma.

A second method to stabilize the flute mode is to apply feedback voltages to segmented, end plates in contact with the plasma. In principle, such "axial feedback stabilization" does not lead to enhanced electron heat loss to the end plates. Experiments in a low temperature, multiple mirror plasma confinement device have demonstrated the stabilization of the $m=1$ flute mode using axial feedback to an endplate split into four sectors [14]. For this device, the escaping core plasma density near the end plates was of the order of the confined density in the midplane of the device, yielding a high sheath admittance and good coupling of the feedback system to the plasma. Axial feedback stabilization of a hot, mirror confined core plasma has been studied theoretically [15,16]. For such a plasma, the escaping core plasma density is very low, such that the sheath admittance is low and good coupling of the feedback voltages directly to the core plasma is difficult to achieve. Voltages have been applied to segmented end plates in tandem mirror devices to successfully control nonambipolar radial transport [17,18]. This suggests that sufficiently strong coupling can be achieved to use axial feedback stabilization in these devices.

In the present study, we examine theoretically the stabilization of the flute mode in a tandem mirror device by applying feedback voltages to an annular endplate split into four sectors, having arbitrary inner and outer radii. The endplate is in contact with the escaping halo plasma, thus achieving a high sheath admittance and good feedback coupling to the plasma. In section 2, we derive the relative dielectric constant for the plasma and identify the corresponding circuit elements for the feedback model. In section 3, we represent the confined plasma using a three layer model and obtain the dispersion equation and feedback equation for the system. In section 4, we apply the feedback equation to three, representative, confined plasmas having parameters characteristic of the MFTF-B and TMX-U devices at the Lawrence Livermore National Laboratory and the MMX device at the University of California, Berkeley. We determine the feedback gain required for stabilization and estimate the feedback power required to maintain stabilization in the presence of noise fluctuations in the plasma. In section 5, we discuss the results and limitations of the theory.

2. Single Layer Dispersion Relation and Circuit Representation

We consider a plasma in the slab geometry shown in Fig. 1. The direction of the uniform magnetic field is taken to be the z-direction and $\bar{B}_0 = (0,0,B_0)$. The x-axis is taken in the direction of the density gradient with the positive direction outward from the plasma, so that the pressure is $p_0 = p_0(r)$. The effects of the curvature of the magnetic field-line are represented by the effective gravity $g = v_{th}^2/R_c$, where $R_c = l_B^2/R_p$ is the radius of curvature of the field-line, R_p is the radius of the plasma, and l_B is the mirror scale length.

2.1. The Dispersion Relation

We use the two fluid equations and the Poisson's equation as follows:

$$\frac{d_s n_s}{dt} + n_s \nabla \cdot \vec{u}_s = S_s , \tag{1}$$

$$\nabla^2 \phi = -\sum_s \frac{q_s n_s}{\epsilon_o} , \tag{2}$$

where

$$\frac{d_s}{dt} \equiv \frac{\partial}{\partial t} + \vec{u}_s \cdot \nabla , \tag{3}$$

ϕ is the perturbed potential, and the subscript s represents the species s. The feedback source terms S_s are given by [15,19]

$$S_e = -\frac{y_e(\omega)}{e l_T}\phi , \tag{4}$$

$$S_i = 0 , \tag{5}$$

where, l_T is the half length of the confined plasma, and $y_e(\omega)$ is the admittance per unit area of the external sheath. By neglecting the viscous terms of the pressure tensor, we have the momentum balance equation

$$n_s m_s \frac{d_s \vec{u}_s}{dt} = -\nabla p_s + q_s n_s (\vec{E} + \vec{u}_s \times \vec{B}) + n_s m_s \vec{g}_s + \vec{\delta}_c . \tag{6}$$

The collision term $\vec{\delta}_c$ is given by

$$\vec{\delta}_s = \frac{q_s}{e} n_e m_e \nu_{ei} (\vec{u}_e - \vec{u}_i) , \tag{7}$$

where ν_{ei} is the electron-ion collision frequency. Neglecting the flow velocity due to classical diffusion, we have the equilibrium flow velocities

$$\vec{u}_{os} = -\frac{g_s}{\Omega_s}\hat{y} - \frac{T_s n_o'}{n_o m_s \Omega_s}\hat{y} , \tag{8}$$

where, $n_0' = |dn_0/dx|$, T_s is the temperature, and $\omega_s = q_s B/m_s$ is the gyrofrequency for each species s. We linearize (1-7) under the assumptions that $T_e \simeq T_i$, $\Omega_i \ll |\Omega_e|$, $\rho_i/R_p \ll 1$, $|\vec{u}_{1i}| \ll |\vec{u}_{1e}|$, and the perturbation is of the form $e^{i(ky-\omega t)}$. Here ρ_i is the ion gyroradius. The convective derivative (3) can be written as

$$\frac{d_s}{dt} = -i(\omega - \omega_s^* - \omega_{gs}^*)$$

$$\equiv -i\omega_s ,$$

where ω_s^* is the diamagnetic drift frequency

$$\omega_s^* = -\frac{kT_s}{m_s\Omega_s}\frac{n_o'}{n_o} ,$$

and ω_{gs}^* is the gravitational drift frequency, defined as

$$\omega_{gs}^* \equiv -\frac{kg_s}{\Omega_s} .$$

The perturbed pressure equation is given by

$$p_{is} = -\frac{1}{i\omega_s}(-\vec{u}_{is}\cdot\nabla p_{os} - \gamma p_{os}\nabla\cdot\vec{u}_{1s}) \tag{9}$$

Keeping only the convected plasma pressure fluctuations [the $\nabla\cdot\vec{u}_{1s}$ term yields negligible corrections (see Appendix A)] in the above expression we find

$$p_{1s} = \frac{1}{i\omega_s}\vec{u}_{1s}\cdot\nabla p_{os} \tag{9'}$$

Now using (9') for the perturbed pressure, and neglecting the inertia for electrons and the collision term for ions in Eq. (6), we have the following linearized momentum balance equations;

$$\frac{i\vec{k}e\phi_1}{m_e} + \frac{\vec{k}}{\omega_e}\frac{n_o'}{n_o}\frac{T_e}{m_e}u_{1e}^x + \Omega_e\vec{u}_{1e}\times\hat{z} - \nu_{ei}\vec{u}_{1e} = 0 \tag{10}$$

$$-i\omega_i\vec{u}_{1i} = -\frac{i\vec{k}e\phi_1}{m_i} + \frac{\vec{k}}{\omega_i}\frac{n_o'}{n_o}\frac{T_i}{m_i}u_{1i}^x + \Omega_i\vec{u}_{1i}\times\hat{z} \tag{11}$$

Solving (10) and (11) for the perturbed velocities, we have

$$u_{1e}^x \simeq \frac{ike\phi_1}{m_e\Omega_e(1+\frac{\omega_e^*}{\omega_e})} \tag{12}$$

$$u_{1e}^y \simeq \frac{ik\nu_{ei}e\phi_1}{m_e\Omega_e^2(1+\frac{\omega_e^*}{\omega_e})} \tag{13}$$

$$u_{1i}^x \simeq -\frac{ike\phi_1}{m_i\Omega_i(1+\frac{\omega_i^*}{\omega_i})} \tag{14}$$

$$u_{1i}^y \simeq -\frac{ke\phi_1\omega_i}{m_i\Omega_i(1+\frac{\omega_i^*}{\omega_i})} \tag{15}$$

Inserting (12-15) into the linearized continuity equations, we find the perturbed densities

$$(\frac{n_1}{n_o})_e = \frac{\omega_e^*}{\omega-\omega_{ge}^*}\frac{e\phi_1}{T_e} + \frac{ik^2\nu_{ei}}{m_e\Omega_e^2}\frac{T_e}{\omega-\omega_{ge}^*}\frac{e\phi_1}{T_e} + \frac{iy_e(\omega)}{n_oe^2l_T}\frac{T_e}{\omega_e}\frac{e\phi_1}{T_e}, \tag{16}$$

$$(\frac{n_1}{n_o})_i = -\frac{\omega_i^*}{\omega-\omega_{gi}^*}\frac{e\phi_1}{T_i} - b_i\frac{\omega_i}{\omega-\omega_{gi}^*}\frac{e\phi_1}{T_i}, \tag{17}$$

where $b_i \equiv (k^2\rho_i^2)$

We now determine the plasma dielectric function (see Appendix B for further details). Poisson's equation (2) can be rewritten as

$$-k^2\kappa\phi = -k^2\phi + \frac{e}{\epsilon_o}(n_{1i} - n_{1e}). \tag{18}$$

where, κ is the relative dielectric constant. Noting that

$$\omega^* \equiv \omega_e^* = -\omega_i^*$$

$$\omega_g^* \equiv \omega_{ge}^* = -\omega_{gi}^*$$

for $T_e \simeq T_i \simeq T$, and that $\kappa \gg 1$, $|\omega_g^*| \ll |\omega|$, and $|\omega^*| \ll |\omega|$ for the plasma that we consider, we identify κ as

$$\kappa = \frac{e^2 n_o}{k^2 \epsilon_o T} \frac{1}{\omega^2 - \omega_g^{*2}} (2\omega^* \omega_g^* + \frac{ik^2 \nu_{ei} T}{m_e \Omega_e^2} (\omega + \omega_g^*)$$
$$+ \frac{i y_e(\omega) T}{n_o e^2 l_T} (\omega + \omega_g^*) + b_i (\omega + \omega^* + \omega_g^*)(\omega - \omega_g^*))$$
$$\approx \frac{e^2 n_o}{k^2 \epsilon_o T} b_i ((1 + \frac{\omega^*}{\omega}) + (\frac{k^2 \nu_{ei} T}{m_e \Omega_e^2 b_i} + \frac{y_e T}{n_o e^2 l_T b_i}) \frac{i}{\omega} + \frac{2\omega^* \omega_g^*}{b_i \omega^2}) . \quad (18')$$

The first term represents the polarization drift effect modified by the diamagnetic drift, the second term represents the collisional effect, the third term represents the line-tying effect through the external sheath, and the last term represents the $\vec{g} \times \vec{B_0}$ curvature drift effect. By putting $\nu_{ei} = 0$ and $y_e = 0$, we recover the usual noncollisional dispersion relation [3,20-21]

$$\omega^2 + \omega^* \omega + \gamma_{MHD}^2 = 0 \quad (19)$$

where $\gamma_{MHD}^2 = g/R_p$ is the ideal MHD plasma growth rate. We note that the $m = 1$ mode is not rigid for a diffuse boundary plasma, and the FLR term $\omega^* \omega$ is present even for $m = 1$ due to the finite pressure gradients in the system [3,21].

2.2. Circuit Representation

We now identify the corresponding circuit representations of the plasma by calculating the total external current to the dielectric medium;

$$J_{tot}^{ext} = -\int \nabla \cdot \vec{J} dv = \int \frac{\partial \rho}{\partial t} dv$$
$$= -i\omega \kappa \epsilon_o k^2 A_p l_T \phi \quad (20)$$
$$\equiv (sC_o(1 + \frac{\omega^*}{\omega}) + Y_R + Y_e + \frac{1}{sL}) \phi$$

where A_p is the area of the plasma cross section ,

$$s = -i\omega ,$$
$$C_o = \frac{\epsilon_o k^2 A_p l_T \omega_{pi}^2}{\Omega_i^2} , \quad (21)$$
$$L_p^{-1} = -2 \frac{\epsilon_o k^2 A_p l_T \omega_{pi}^2 \rho_i^2}{R_c R_p} , \quad (22)$$
$$Y_R = \frac{\epsilon_o k^2 A_p l_T \omega_{pi}^2 \nu_{ei}}{\Omega_i \Omega_e} , \quad (23)$$
$$Y_e = y_e A_p . \quad (24)$$

The physical meaning of each of these elements is explained in Vandegrift [16]. Briefly, C_0 is the

capacitance seen across the flute surface, $L < 0$ is the inductance driving the flute mode, Y_R is the transverse collisional conductance, and Y_e is the line-tying admittance. The first term on the right hand side of (20) is the admittance of the capacitance modified by a finite rotational frequency ω^*. These circuit elements (21)-(24) give a convenient interpretation for the physical process of the flute instability. A random fluctuation of the plasma induces a current in the R - L - C parallel resonant circuit resulting in a charge on the capacitor. The quality factor Q of the resonance circuit is decreased by increasing Y_R and Y_e. These shunted resistors try to discharge the separated charges, giving a reduced growth rate $\gamma < \gamma_{MHD}$. With Y_R and $Y_e = 0$, the system is stable provided $\gamma_{MHD} < \omega^*/4$.

3. Feedback Model and Modified Dispersion Relation

Figure 2 shows the three layer model for the mirror confined plasma that we consider here. Regions I-IV represent the core plasma, the transition plasma, the external halo plasma, and the surrounding vacuum region, respectively. The transition plasma (region II) couples the core plasma (region I) to the halo plasma (region III), on which the feedback signal is applied axially through segmented annular feedback plates located at the end of the machine.

3.1. Flute Mode in Radially Layered Plasma

For the $m = 1$ flute mode, in cylindrical coordinates, we represent the perturbed potential ϕ, which vanishes at $r = \infty$, as

$$\begin{aligned} \phi_p &= Ar\cos\theta, \\ \phi_t &= Br\cos\theta + \frac{C}{r}\cos\theta, \\ \phi_h &= Dr\cos\theta + \frac{E}{r}\cos\theta, \\ \phi_v &= \frac{F}{r}\cos\theta. \end{aligned} \tag{25}$$

Enforcing the boundary conditions on (25), i.e., that ϕ and the normal component of the electric displacement $\overline{D}$ be continuous across the boundary, and assuming that the dielectric constants for the plasma are much greater than the vacuum ($\kappa_p, \kappa_t, \kappa_h \gg 1$) we obtain the dispersion relation as

$$(\kappa_p+\kappa_t)(\kappa_t-\kappa_h)\frac{1}{R_p^2R_h^2}-(\kappa_t-\kappa_p)(\kappa_t+\kappa_h)\frac{1}{R_t^2R_h^2}$$

$$+(\kappa_p+\kappa_t)(\kappa_t+\kappa_h)\frac{1}{R_t^2R_p^2}-(\kappa_t-\kappa_p)(\kappa_t-\kappa_h)\frac{1}{R_t^4}=0 \tag{26}$$

where, R_p, R_t, and R_h are the radii of the core, transition, and halo boundaries, respectively. The relative dielectric constants κ_p, κ_t, and κ_h are given by (18). Assuming that the core temperature is much higher than the transition or halo temperature, we have

$$\kappa_p=\frac{\omega_{pi}^{I2}}{\Omega_i^2}\left(1+\frac{\omega_I^*}{\omega}+\frac{i}{\omega}\frac{k^2\nu_{ei}^I T^I}{m_e\Omega_e^2 b_i^I}+\frac{2\omega_I^*\omega_{gI}^*}{b_i^I\omega^2}\right), \tag{27}$$

$$\kappa_t=\frac{\omega_{pi}^{II2}}{\Omega_i^2}\left(1+\frac{\omega_{II}^*}{\omega}+\frac{i}{\omega}\frac{k^2\nu_{ei}^{II}T^{II}}{m_e\Omega_e^2 b_i^{II}}\right), \tag{28}$$

$$\kappa_h=\frac{\omega_{pi}^{III2}}{\Omega_i^2}\left(1+\frac{\omega_{III}^*}{\omega}+\frac{i}{\omega}\frac{k^2\nu_{ei}^{III}T^{III}}{m_e\Omega_e^2 b_i^{III}}+\frac{y_eT^{III}}{n_o^{III}e^2l_Tb_i^{III}}\right), \tag{29}$$

Here, we have neglected the curvature driven effects for the transition and halo regions, and considered the line-tying effect only for the halo region.

A typical tandem mirror geometry is shown in Fig. 3. The bad curvature drive is concentrated mainly in the plug region having characteristic length l_p. For this geometry, the average radius of curvature R_c is $(l_B^2l_T)/(R_pl_p)$. By using (27)-(29). and calculating the external current for each region, we have

$$Y_p=sC_{po}\left(1+\frac{\omega_I^*}{\omega}\right)+Y_{Rp}+\frac{1}{sL_p}, \tag{30}$$

$$Y_t=sC_{to}\left(1+\frac{\omega_{II}^*}{\omega}\right)+Y_{Rt}, \tag{31}$$

$$Y_h=sC_{ho}\left(1+\frac{\omega_{III}^*}{\omega}\right)+Y_{Rh}+Y_{he}, \tag{32}$$

where, Y_p, Y_t, and Y_h are the effective admittances, and A_p, A_t, and A_h are the areas of the core, transition, and halo plasmas, respectively,

$$C_{po} = \frac{\epsilon_o k^2 A_p l_T \omega_{pi}^{I^2}}{\Omega_i^2}, \qquad Y_{Rp} = \frac{\epsilon_o k^2 A_p l_T \omega_{pi}^{I^2} \nu_{ei}^{I}}{\Omega_e \Omega_i},$$

$$L_p^{-1} = -2\epsilon_o k^2 A_p l_T \omega_{pi}^{I^2} \frac{\rho_i^2}{R_c R_p}, \qquad C_{to} = \frac{\epsilon_o k^2 A_t l_T \omega_{pi}^{II^2}}{\Omega_i^2},$$

$$Y_{Rt} = \frac{\epsilon_o k^2 A_t l_T \omega_{pi}^{II^2} \nu_{ei}^{II}}{\Omega_e \Omega_i}, \qquad C_{ho} = \frac{\epsilon_o k^2 A_h l_T \omega_{pi}^{III^2}}{\Omega_i^2},$$

$$Y_{Rh} = \frac{\epsilon_o k^2 A_h l_T \omega_{pi}^{III^2} \nu_{ei}^{III}}{\Omega_e \Omega_i}, \qquad \textit{and} \qquad Y_{he} = y_e^{III} A_h.$$

By multiplying (26) by $(s\epsilon_o k^2 A_p l_T)^2$, and using (30-32), we can rewrite the dispersion relation without feedback in terms of the circuit elements as

$$Y_p Y_h + Y_t Y_h \frac{R_p^2}{(R_t^2 - R_p^2)^2}(R_p^2 + R_t^2) + Y_t^2 \frac{R_p^2(R_h^2 + R_t^2)}{(R_t^2 - R_p^2)^2} + Y_p Y_t \frac{(R_t^2 + R_h^2)(R_t^2 + R_p^2)}{(R_t^2 - R_p^2)^2} = 0. \tag{33}$$

3.2. Circuit Representation without Feedback

Now, we consider the equivalent circuit representation of the above dispersion relation in Fig. 4a. Taking the input impedance seen at the core-transition boundary $Y_{in} = 0$ (resonance), we obtain

$$Y_p Y_h + (\alpha + \beta) Y_t Y_h + (\alpha\beta + \beta\gamma + \alpha\gamma) Y_t^2 + (\beta + \gamma) Y_t Y_p = 0. \tag{34}$$

Comparing (33) with (34), we can recover the dispersion relation by setting

$$\alpha + \beta = \frac{R_p^2(R_p^2 + R_t^2)}{(R_t^2 - R_p^2)^2}, \tag{35}$$

$$\beta + \gamma = \frac{(R_t^2 + R_h^2)(R_t^2 + R_p^2)}{(R_t^2 - R_p^2)^2}, \tag{36}$$

$$\alpha\beta + \beta\gamma + \alpha\gamma = \frac{R_p^2(R_h^2 + R_t^2)}{(R_t^2 - R_p^2)^2}. \tag{37}$$

Solving for α, β, γ, we obtain

$$\alpha = \frac{R_p^2(R_p^2 + R_t^2)}{(R_t^2 - R_p^2)^2} - \beta, \tag{38}$$

$$\beta = \frac{2R_p^2 R_t (R_t^2 + R_h^2)^{1/2}}{(R_t^2 - R_p^2)^2}, \tag{39}$$

$$\gamma = \frac{(R_t^2 + R_h^2)(R_t^2 + R_p^2)}{(R_t^2 - R_p^2)^2} - \beta, \tag{40}$$

(For typical parameters of MFTF-B, $\alpha \sim -3$, $\beta \sim 5$, $\gamma \sim 8$). the form of these coupling coefficients implies the following: i) The effective capacitance of the core plasma is decreased because charge cancellation occurs at the boundary with the transition plasma. ii) If the halo plasma is perfectly line-tied, i.e., $Y_{he} \rightarrow \infty$, the effective capacitance due to the transition and the halo plasma is about $2C_t < C_p$. Thus, the growth rate of the flute instability is somewhat reduced due to the increased inertia of the system. But there is no circuit element which provides $L > 0$ that can compensate $L_p < 0$ to obtain complete stability. iii) If we provide a positive inductance by feedback, we might have stability. iv) Note that the system cannot be driven into instability by the form of the coupling coefficients alone, even if $\alpha < 0$ because the equivalent circuit representation has not introduced any new physics. This can be seen by calculating the total capacitance of the system with $L_p = 0$, ω^*'s = 0 and $Y_{he} = 0$.

$$C_{tot} = C_p + \alpha C_t + \frac{\beta\gamma'}{\beta + \gamma'} C_t > 0,$$

where $\gamma' = (\gamma C_t + C_h)/C_t > \gamma$.

3.3. Circuit Representation with Feedback

Now we consider an equivalent circuit model with feedback. With feedback voltage applied at the halo shaped feedback plates located at the end of the machine, the lower terminal of the line-tying admittance is forced away from system ground. So, we can represent the equivalent circuit model of the system as shown in Fig. 4b, where $Y_1 \equiv Y_h - Y_{he}$. By considering $Y_{in} = 0$, we obtain the dispersion relation with feedback:

$$Y_p + \alpha Y_t + \frac{\beta Y_t(\gamma Y_t + Y_h)}{(\beta + \gamma)Y_t + Y_h} + \frac{\beta Y_t \eta Y_{he}}{(\beta + \gamma)Y_t + Y_h} = 0 \tag{41}$$

where η is the voltage transfer function of the feedback network. We can analyze this problem with more general feedback theory, but for simplicity, we consider the regulator problem with $e_i = 0$ ($e_i \neq 0$ corresponds to an external driving signal). If we choose the feedback transfer function $\eta(s)$ as

$$\eta(s) = -\frac{G}{sL_p}\frac{(\beta+\gamma)Y_t + Y_h}{\beta Y_t Y_{he}}, \tag{42}$$

the negative inductance included in Y_p in (41) cancels out for $G = 1$, and the system becomes stable. The feedback network of (42) can be realized with two strictly proper stable networks. For simplicity, we neglect Y_{Rp}, Y_{Rt}, and Y_{Rh} and assume $\omega^*_{III} = 0$. then, (42) becomes

$$\begin{aligned}\eta(s) &= \frac{G}{s|L_p|}\frac{(\beta+\gamma)(sC_{to}+Y_{t\phi}) + sC_h + Y_{t\phi} + Y_{he}}{\beta(sC_{to}+Y_{t\phi})Y_{he}} \\ &= \frac{e_{fb}}{e_p},\end{aligned} \tag{43}$$

where e_{fb} is the feedback voltage applied at the feedback plate, and $Y_{t\phi}$ is defined by

$$Y_{t\phi} = sC_{to}\frac{\omega^*_{II}}{\omega} = -j\omega^*_{II}C_{to}$$

We introduce an auxiliary variable e_1 to realize $\eta(s)$ as

$$\begin{aligned}e_1 &= \left[A + \frac{G(Y_{t\phi}+Y_{he})}{s}\right]e_p \\ &\equiv -H_1(s)e_p\end{aligned} \tag{44}$$

with

$$A \equiv G[(\beta+\gamma)C_{to} + C_h]\,.$$

Then, we have

$$\begin{aligned}e_{fb} &= -\frac{1}{s\beta|L_p|Y_{he}C_{to} + \beta|L_p|Y_{he}Y_{t\phi}}e_1 \\ &\equiv H_2(s)e_1\end{aligned} \tag{45}$$

and realize $\eta(s)$ with two proper stable networks $H_1(s)$ and $H_2(s)$ which are schematically given by Figs. 5a and 5b. (Note that $Y_{t\phi}$ can be realized by 90° spatially rotated signals.)

We now consider the sensitivity of the system stability in realizing the feedback transfer function $\eta(s)$. The circuit of Fig. 4b can be redrawn as Fig. 4c. Here the negative inductance L_p is separated

from the rest of the circuit Y_4 which is a passive network, and the feedback effect is represented by an equivalent feedback admittance Y_{fb}. The passive network Y_4 and the feedback admittance Y_{fb} are given by

$$Y_{fb} = \frac{\eta(s)\beta Y_t Y_{he}}{Y_h + (\beta+\gamma)Y_t}, \tag{46}$$

$$Y_4 = Y_p + \frac{1}{s|L_p|} + \alpha Y_t + \frac{(Y_h + \gamma Y_t)\beta Y_t}{Y_h + (\beta+\gamma)Y_t}. \tag{47}$$

For the system to be stable, we require that Y_{fb} cancel the negative inductance L_p. The time delay effects in the feedback network can be represented by introducing a constant phase shift θ in the complex gain G, i.e., $G = |G|e^{i\theta}$. Then, for stability the feedback admittance should be

$$Y_{fb} = \frac{G}{s|L_p|} = \frac{|G|cos\theta}{s|L_p|} + \frac{|G|sin\theta}{\omega|L_p|}$$

and we need

$$|G| \geq \frac{1}{cos\theta}, 0 \leq \theta < \frac{\pi}{2} \tag{48}$$

for the system stability. The condition (48) for stability does not seriously restrict the choice of $\eta(s)$. It can also be shown that the other mismatches of the parameters in $\eta(s)$ do not yield any serious restrictions in designing $\eta(s)$. For example, a mismatch in $Y = Y_t$, Y_h or Y_{he} requires the feedback gain to be $G > 1 + |\Delta Y/Y|$. Thus, the feedback realization (42) gives quite robust stability for $G > 1$.

In the next section, we examine the behavior of the roots of the dispersion-relation (41) which are obtained by setting the numerator to zero:

$$\begin{aligned}
&s^3\left(L'_p(C_{ho}+(\beta+\gamma)C_{to})(C_{po}+(\alpha+\beta)C_{to}) - \beta^2 C_{to}^2 L'_p\right) \\
+&s^2\Big(L'_p(C_{po}+(\alpha+\beta)C_{to})((\beta+\gamma)(Y_{t\phi}+Y_{Rt})+Y_{h\phi}+Y_{he}+Y_{Rh}) \\
&\quad + L'_p(C_{ho}+(\beta+\gamma)C_{to})((\alpha+\beta)(Y_{t\phi}+Y_{Rt})+Y_{Rp}+Y_{R\phi}) \\
&\quad - 2\beta^2 L'_p C_{to}(Y_{t\phi}+Y_{Rt})\Big)
\end{aligned}$$

$$
\begin{aligned}
&+s\Big((G-1)((\beta+\gamma)C_{to}+C_{ho})-\beta^2(Y_{t\phi}+Y_{Rt})^2L'_p \\
&\quad +L'_p((\alpha+\beta)(Y_{t\phi}+Y_{Rt})+Y_{Rp}+Y_{p\phi}) \\
&\quad ((\beta+\gamma)(Y_{t\phi}+Y_{Rt})+Y_{h\phi}+Y_{he}+Y_{Rh})\Big) \\
&+\ (G-1)((\beta+\gamma)(Y_{t\phi}+Y_{Rt})+Y_{h\phi}+\ Y_{he}+Y_{Rh}) \\
&=0
\end{aligned}
\tag{49}
$$

4. The Results of Feedback

We apply the results of the previous section to parameters and geometry characteristic of the TMX-U, the MFTF-B and the MMX experiments. The typical parameters and corresponding values of the circuit elements are given in Table 1 and Table 2, respectively.

4.1 Solution of the Dispersion Relation with Feedback

We assume that the density is constant with radius except in the transition region where it decreases with a constant slope. (Thus ω_s^* exists only in the transition region.) For the line-tying admittance, we use the Kunkel and Guillory model [19] for Y_{he}, i.e.,

$$
Y_e^{III}=\frac{1}{4}\,\frac{\varepsilon_0 v_{thi}^{III}}{(\lambda_{De}^{III})^2} \tag{50}
$$

where λ_{De} is the electron Debye length, and v_{thi} is the ion thermal velocity. Particle simulation results for the sheath characteristic show that this linear model for the sheath impedance gives a good description of the coupling of the halo plasma to the feedback plate, provided the voltage across the sheath is less than approximately 40% of the thermal plasma potential [22]. By putting the numerical values for the circuit elements into (49), and solving for the roots of the polynomial with G as a parameter, we obtain Figs. 6-8, the root loci of (49) for MMX, TMX-U, and MFTF-B, respectively. Note Re(s) < 0 (roots in the left half plane) for stability. We choose the MMX experiment (Fig. 6) to describe the behavior of the roots. Without feedback, G = 0, we have three roots; root 1 at (-5.74×10^5, 1.98×10^5), root 2 at (6.04×10^4, 4.38×10^3), root 3 at (-4.00×10^5, 2.90×10^4). Root 2 is the flute unstable root that must be stabilized by feedback. Root 3 is the stable conjugate root of 2. The stable

root 1 arises from the $R_{he}C_{eff}$ time constant of the system, which can easily be seen from the high frequency limit of (49). It is clear that for $G \geq 1.0$, the flute mode is stabilized. Similar behavior is seen for TMX-U and MFTF-B.

Two interesting limiting cases are $A_t \to 0$, $G \to 0$ i.e., the "surface line-tying" model [7-13], and $R_t \to R_h \gg R_p$. For the case of $A_t \to 0$ and $G \to 0$, we obtain the voltage transfer ratio for the circuit in Fig. 4a,

$$\begin{aligned} \frac{e_p}{e_h} &= \frac{\beta Y_t}{Y_p + (\alpha+\beta)Y_t} \\ &= \frac{2R_p^2 R_t (R_t^2 + R_h^2)^{1/2} Y_t}{(R_t^2 - R_p^2)^2 Y_p + R_p^2 (R_p^2 + R_t^2) Y_t} \\ &\to (1 + \frac{R_h^2}{R_p^2})^{1/2} \qquad as \qquad R_t \to R_p, \qquad i.e., \qquad A_t \to 0 \end{aligned} \tag{51}$$

If $Y_{he} \to \infty$, the core plasma is shorted out by the perfect line-tying, and the system is stabilized.

In the other limiting case of $R_t \to R_h \gg R_p$, we obtain

$$\frac{R_p^2}{R_p^2 + R_h^2} \kappa_t R_t^2 + \kappa_p R_p^2 \approx (\kappa_t + \kappa_p) R_p^2 = 0; \tag{52}$$

i.e., $\kappa_t + \kappa_p = 0$, which is physically equivalent to the case of a core plasma surrounded by an infinite external plasma. For $\kappa_t = \kappa_{vac} = 1$, we have a system consisting of a core plasma only.

4.2. Feedback Power Requirement

We now consider the feedback power necessary to stabilize the m = 1 flute mode. The level of this required power will clearly determine the viability of this stabilization scheme. There will always be some wideband plasma noise in which the coherent flute mode will be embedded in any machine. The sensors will detect both the noise and the coherent fluctuation, and the feedback signal will be composed of processed versions of these. The required feedback power will therefore be proportional to the noise power in the plasma.

We use circuit simulation codes; e.g., SPICE, to determine the required feedback power for the circuit of Fig. 5a, which is schematically redrawn in Fig. 9 with the circuit elements explicitly shown. We first choose a thermal noise source e_n' associated with the cross field core resistance R_{core} and later we rescale the results to account for a more realistic, nonthermal fluctuation level. For

thermal fluctuations, the fluctuation voltage spectrum is given by

$$e_n(\omega) = \frac{e_n'}{(BW)^{1/2}} \tag{53}$$

where,

$$e_n = (4KTR_{core}BW)^{1/2}\text{volts}\ , \tag{54}$$

$R_{core} = 1/Y_{RP}$, KT is the temperature of the core in joules, e_n' is the rms thermal fluctuation voltage, and BW is the band-width of the feedback system. For each machine that we consider, the normalized real power spectra of the core plasma and feedback circuit to the thermal fluctuation with G = 1.5 are plotted in Fig. 10 for MMX, Fig. 11 for TMX-U, and Fig. 12 for MFTB-B. In these figures, $P_p = \frac{1}{2}\ |e_p|^2\ \text{Re}\ [Y_p]$ and $P_{he} = \frac{1}{2}\ |e_{he}|^2 Y_{he}$. Note that the fluctuation power spectrum in the core is centered at γ_{MHD}, even though we use a thermal spectrum for $e_n(\omega)$. The feedback power has a roughly constant spectrum for $\omega \leq \gamma_{MHD}$ and then is sharply decreasing. The sharp peak in the MFTF-B spectrum is due to the low collisionality of the core and transition plasma. Given the core plasma voltage spectrum for $e_n(\omega)$, we can estimate the rms plasma centroid radial displacement of the core from the formula for the $\vec{E} \times \vec{B}$ drift motion. The estimated rms plasma displacement for the thermal noise is

$$\begin{aligned} \xi_{rms} &\simeq \left(\int_o^{BW} \left(\frac{e_p(\omega)}{\omega B R_p}\right)^2 d\omega\right)^{1/2} \\ &\sim 5.56 \times 10^{-10}\ [m]\ \text{for MMX} \\ &2.45 \times 10^{-11}\ [m]\ \text{for TMX} - \text{U} \\ &4.10 \times 10^{-12}\ [m]\ \text{for MFTF} - \text{B} \end{aligned} \tag{55}$$

Here, we have chosen the band-width of the feedback system to be 10^8 rad/sec. Since $e_p(\omega)$ falls sharply for $\omega > \gamma_{MHD}$, the results are not sensitive to the choice of bandwidth provided $BW \gg \gamma_{MHD}$. The power supplied by the feedback system is calculated from the standard formula

$$P_{fb} = \int_o^{BW} \eta(\omega) e_p(\omega) \cdot I_{fb}^*(\omega) d\omega\ , \tag{56}$$

where $I_{fb}^*(\omega)$ is the complex conjugate of the current flowing at the output port of the feedback system.

The real and reactive powers are given by

$$\begin{aligned}
\mathrm{Re}\,[P_{fb}] &\sim 1.38 \times 10^{-11}\,[W] \text{ for MMX} \\
&\quad 5.94 \times 10^{-16}\,[W] \text{ for TMX} - \mathrm{U} \\
&\quad 3.71 \times 10^{-11}\,[W] \text{ for MFTF} - \mathrm{B} \\
\mathrm{Im}\,[P_{fb}] &\sim 9.47 \times 10^{-14}\,[W] \text{ for MMX} \\
&\quad 3.92 \times 10^{-16}\,[W] \text{ for TMX} - \mathrm{U} \\
&\quad 3.26 \times 10^{-10}\,[W] \text{ for MFTF} - \mathrm{B}
\end{aligned} \tag{57}$$

Of course, the m = 1 flutelike fluctuations in real devices are not at thermal levels. We therefore rescale the rms plasma centroid displacement ξ_{rms} to a reasonable level that can be detected and controlled by a practical feedback system. We choose $\xi_{rms}/R_p \approx 1\%$. Since $P_{fb} \propto \xi_{rms}^2$, we obtain, using (55) and (57), the result

$$\begin{aligned}
\mathrm{Re}[P_{fb}] &\sim 1.8\,[W] \text{ for MMX} \\
&\quad 4.0\,[W] \text{ for TMX} - \mathrm{U} \\
&\quad 20.\,[MW] \text{ for MFTF} - \mathrm{B} \\
\mathrm{Im}[P_{fb}] &\sim 1.2\times 10^{-3}\,[W] \text{ for MMX} \\
&\quad 2.6\,[W] \text{ for TMX} - \mathrm{U} \\
&\quad 170\,[\mathrm{MW}] \text{ for MFTF} - \mathrm{B}
\end{aligned} \tag{58}$$

These numerical results may be compared with a rough estimation of required reactive feedback power for a single layer model, calculated from the perturbed plasma energy δW_s, for a given perturbed displacement ξ, that is discharged in the time interval of $1/\gamma_{MHD}$. For a uniform plasma pressure P_0 within radius R_p, the perturbed energy is given by

$$\delta W_s = \frac{1}{2}\int (\vec{\xi}\cdot\hat{n})^2 \left[\nabla\left(P + \frac{B^2}{2\mu_o}\right)\right]\cdot d\vec{S} \tag{59}$$

with

$$P(r) = P_o,\ r < R_p\ ;$$

$$0,\ r > R_p\ .$$

Using following relations;

$$d\vec{S}\cdot\nabla = 2\pi\ell_p r dr\frac{\partial}{\partial r}\ ,$$

$$\frac{\partial}{\partial r}\left(\frac{B^2}{2\mu_o}\right)\Bigg|_{R_p^-}^{R_p^+} \approx \frac{B_{vac}^2}{\mu_o R_c} - \frac{B^2}{\mu_o R_c} = \frac{2P}{R_c}\ ,$$

$$R_c = \frac{\ell_B^2}{R_p}\frac{\ell_T}{\ell_p}\ ,$$

we obtain the perturbed energy from (59) as

$$\delta W_s \approx P_o V \xi^2/\ell_B^2 \tag{60}$$

where V is the volume of plasma in the plug. Assuming that the perturbed energy δW_s is discharged in the time interval $1/\gamma_{MHD}$, we have the power required to stabilize the system

$$\begin{aligned} P \approx & \gamma_{MHD}\delta W_s \approx \frac{v_{thi}}{\ell_B}\left(\frac{\ell_p}{\ell_T}\right)^{1/2} P_o V\frac{\xi^2}{\ell_B^2} \\ & \propto \frac{n_o\xi^2 T^{3/2}\ell_p^{3/2}R_p^2}{\ell_B^3\ell_T^{1/2}} \\ & \sim 6.8\times 10^{-4}\ [\,W\,] \text{ for MMX} \\ & \qquad 2.1\ [\,W\,] \text{ for TMX}-\text{U} \\ & \qquad 5.7\ [\,MW\,] \text{ for MFTF}-\text{B} \end{aligned} \tag{61}$$

These simple estimates of the power requirement for a single layer model (Eq. (61)) agree well with our intuition that the larger experiment requires more feedback power to stabilize. For MMX and TMX-U, the estimated reactive powers from (58) and (61) give a reasonable agreement. For the low temperature, highly resistive MMX plasma, the real power greatly exceeds the reactive power. However, the three layer model predicts approximately 30 times larger reactive power for MFTF-B than that predicted from a single layer model because of poor coupling between the core and the halo plasma; namely, $\beta\omega C_{to} \ll Y_{he}$ for MFTF-B. For the three layer model with large Y_{he} (poor coupling) and $C_p \gg C_t, C_h$, the feedback power scales with

$$P_{fb} \propto \frac{G^2}{\sqrt{G-1}}\frac{n_o\xi^2T^{3/2}\ell_p^{3/2}R_p^2}{\ell_B^3\ell_T^{1/2}}\frac{C_p}{C_t}\frac{\beta+\gamma}{\beta}\ . \tag{62}$$

So, by increasing the mirror curvature scale length l_B and/or putting the inner radius of the feedback plate close to the core plasma and/or decreasing the minimum detectable distance ξ, we can reduce the required power to be handled by a practical feedback system. For example, by increasing l_B from 1m to 3m for MFTF-B while keeping other parameters the same as before, the required feedback power is reduced to Re[P_{fb}] = 0.74 MW, Im[P_{fb}] = 6.4 MW, which is of order of the power that maintains the halo plasma.

5. Discussion and Conclusions

The three layer model analysis of axisymmetric mirror machines shows that we can stabilize the m = 1 flute unstable core plasma by applying proper feedback signals on segmented, annular feedback plates at the end walls. The signals are applied to the feedback plates through the line-tying admittance of the halo plasma sheath. The feedback signals bring appropriate charges to the surface of the core plasma, so as to annul the charges separated by the rigid flute mode and stabilize it. The model ignores finite - β effects and employs sharp boundaries. By increasing the gain G, we have shown that our feedback model can give quite robust stability over the variation of the plasma parameters. However, the plasma parameters change significantly in the initial plasma build-up stage, so that increasing G is impractical. Adaptive identification and tracking of the feedback parameters are essential in the initial plasma build-up stage.

Ther is an advantage to using active feedback on an end ring in contact with the halo plasma, as opposed to modifying the line-tying admittance by employing an emitting end ring. The three layer active feedback model predicts that the flute mode can be suppressed at the core - transition boundary, while the surface line-tying model predicts flute stability only if the ring is in contact with a substantial part of the core plasma. Thus, using an active feedback system with a proper choice of feedback transfer function, we can obtain absolute stability with sufficiently large inner radius of the feedback plates that the plasma end loss heat flux and the radiation or neutron damage on the feedback plates can be held to acceptable levels. The power required by the feedback system to maintain stability for the MMX and TMX-U is modest. For a near reactor grade plasma such as MFTF-B, the required feedback power level can be reduced to an acceptable level by increasing the curvature scale length l_B.

Acknowledgement

This work was supported by Department of Energy Contract DE-ATOE-76ET53059. Helpful discussions with A. J. Lichtenberg and B. I. Cohen are gratefully acknowledged.

References

[1] T. K. Fowler and B. G. Logan, *Comments Plasma Phys. Controlled Fusion*, vol. 2, p. 167 (1977).

[2] D. E. Baldwin and B. G., Logan, *Phys. Rev. Lett*, vol. 43, p. 1318 (1979).

[3] M. N. Rosenbluth, N. A. Krall, and N. Rostoker, *Nuclear Fusion 1962 Supplement, Part 1*, p. 143.

[4] R. Moir (ed.), Lawrence Livermore Laboratory Report UCID-16736 (1975).

[5] M. Wickham and G. G. Vandegrift, *Phys. of Fluids*, vol. 25, p. 52 (1982).

[6] G. G. Vandegrift and G. Timothy, Technical Report 83-71, Dept. of Physics, University of California, Irvine (1983).

[7] G. G. Vandegrift, T. N. Good, and N. Rynn, *Bull. Am. Phys. Soc.*, vol. 28, p. 1048 (1983).

[8] S. Fornaca, Y. Kiwamoto, and N. Rynn, *Phys. Rev. Lett.* vol 42, p. 772 (1979).

[9] S. Fornaca, *Phys. of Fluids*, vol. 26, p. 797 (1983).

[10] D. Segal, *Phys. of Fluids*, vol. 26, p. 2565 (1983).

[11] D. Segal, M. Wickham, and N. Rynn, *Phys. of Fluids*, vol. 25, p. 1485 (1982).

[12] T. N. Good, R. Karim, N. Rynn, and H. R. Thomson, Jr., *Bull. Am. Phys. Soc.*, vol. 29, p. 1302 (1984).

[13] T. N. Good, R. Karim, M. K. Okubo, N. Rynn, and H. R. Thomson, Jr., *Bull. Am. Phys. Soc.*, vol. 30, p. 1380 (1985).

[14] S. L. Wong and M. A. Lieberman, *Plasma Physics*, vol. 20, p. 403 (1978).

[15] M. A. Lieberman and S. L. Wong, *Plasma Physics*, vol. 19, p. 745 (1977).

[16] S. L. Wong, Ph.D. Thesis, Dept. of EECS, University of California, Berkeley (1978); G. G. Vandegrift, Ph.D. Thesis, Dept. of Physics, University of California, Berkeley (1982).

[17] E. B. Hooper, Jr., R. H. Cohen, D. L. Correll, J. M. Gilmore, and D. P. Grubb, *Phys. of Fluids*, vol. 28, p. 3609 (1985).

[18] G. Severn, N. Hershkowitz, B. Nelson, and J. Pew, *Bull. Am. Phys. Soc.*, vol. 28, p. 1202 (1983).

[19] W. K. Kunkel and J. Guillory, 7th International Conference on Phenomena in Ionized Gases, Vol. 2, D. Perovic and D. Tosic (ed.), Belgrade (1965).

[20] K. Miyamoto, "Plasma Physics for Nuclear Fusion," MIT Press, p. 370 (1976).

[21] W. A. Newcomb, *Phys. of Fluids*, vol. 28, p. 505 (1985).

[22] C. K. Birdsall, P. G. Gray, and T. L. Crystal, *Bull. Am. Phys. Soc.*, vol 30, p. 1629 (1985).

[23] S. Ichimaru, "Basic Principles of Plasma Physics," Benjamin/Cummings Pub. Company, Inc., p. 41 (1973).

Appendix A

With the compressional part of the perturbed pressure (the second term of (9)) included in Eq. (9), the linearized momentum balance equations become

$$\frac{i\vec{k}e\phi_1}{m_e}+\frac{\vec{k}}{\omega_e}\frac{n_o'}{n_o}\frac{T_e}{m_e}u_{1e}^x-\frac{ik^2\gamma n_oT_e}{\omega_en_om_e}u_{1e}^y\hat{y}+\frac{k\gamma n_o'T_e}{\omega_en_om_e}u_{1e}^y\hat{x}+\Omega_e\vec{u}_{1e}\times\hat{z}-\nu_{ei}\vec{u}_{1e}=0 \quad (A.1)$$

$$-i\omega_i\vec{u}_{1i}=-\frac{i\vec{k}e\phi_1}{m_i}+\frac{\vec{k}}{\omega_i}\frac{n_o'}{n_o}\frac{T_i}{m_i}u_{1i}^x-\frac{ik^2\gamma n_oT_i}{\omega_in_om_i}u_{1i}^y\hat{y}+\frac{k\gamma n_o'T_i}{\omega_in_om_i}u_{1i}^y\hat{x}+\Omega_i\vec{u}_{1i}\times\hat{z} \quad (A.2)$$

Solving (A.1) and (A.2) for the perturbed velocities, we have

$$u_{1e}^x\simeq\frac{ike\phi_1}{m_e\Omega_e(1+\frac{\omega_e^*}{\omega_e})}$$

$$u_{1e}^y\simeq\frac{ik\nu_{ei}e\phi_1}{m_e\Omega_e^2(1+\frac{\omega^*}{\omega_e})(1-\gamma\frac{\omega^*}{\omega_e})}$$

$$u_{1i}^x\simeq-\frac{ike\phi_1}{m_i\Omega_i(1-\frac{\omega^*}{\omega_i})}$$

$$u_{1i}^y\simeq-\frac{ke\phi_1\omega_i}{m_i\Omega_i(1-\frac{\omega^*}{\omega_i})(1+\gamma\frac{\omega^*}{\omega_i})}$$

Then, the perturbed density equations become

$$(\frac{n_1}{n_o})_e=\frac{\omega^*}{\omega-\omega_g^*}\frac{e\phi_1}{T_e}+\frac{ik^2\nu_{ei}}{m_e\Omega_e^2}\frac{T_e}{(\omega-\omega_g^*)(1-\gamma\frac{\omega^*}{\omega_e})}\frac{e\phi_1}{T_e}+\frac{iy_e(\omega)}{n_oe^2l_T}\frac{T_e}{\omega_e}\frac{e\phi_1}{T_e} \quad (A.3)$$

$$(\frac{n_1}{n_o})_i=\frac{\omega^*}{\omega+\omega_g^*}\frac{e\phi_1}{T_i}-b_i\frac{\omega_i}{(\omega+\omega_g^*)(1+\gamma\frac{\omega^*}{\omega_i})}\frac{e\phi_1}{T_i} \quad (A.4)$$

Substituting (A.3) and (A.4) into (18) and assuming $T_e\approx T_i\approx T$, $\kappa\gg 1$, $|\omega_g^*|\ll|\omega|$, and $|\omega^*|\ll|\omega|$, we have the same relative dielectric constant κ as given in (18') .

Appendix B

Since the plasma that we consider is nonhomogeneous, using a spatially uniform dielectric tensor $\tilde{\epsilon}(\vec{k},\omega)$ to describe the $m = 1$ flute mode is inappropriate. However, by modeling the plasma with a series of layers and using the boundary condition that the normal component of the electric displacememt $\vec{D}$ is continuous across the boundary, we can effectively describe the nonhomogeneous plasma. Instead of using the dielectric tensor $\tilde{\epsilon}(\vec{k},\omega)$, we use the dielectric response function $\kappa(\vec{k},\omega)$[23], defined by

$$\rho_{tot} = \frac{\rho_{ext}}{\kappa(\vec{k},\omega)}$$

where ρ_{ext} is an externally injected test charge density, and

$$\nabla \cdot \vec{E} = \rho_{tot}/\epsilon_o \,, \qquad (B.1)$$

which yields

$$\epsilon_o \kappa = \frac{\vec{k} \cdot \tilde{\epsilon}(\vec{k},\omega) \cdot \vec{k}}{k^2} \,.$$

For a multi-layer plasma, $\kappa(\vec{k},\omega)$ is constant in each region, and we can rewrite the Poisson's equation (B.1) as

$$\nabla \cdot (\kappa \vec{E}) = \rho_{ext}/\epsilon_o$$

Then, we have

$$\epsilon_o k^2 \kappa \phi = \rho_{ext} \qquad (B.2)$$

which is the same form as the Poisson's equation in a dielectric medium with dielectric constant $\epsilon_o \kappa$. For a quasi-neutral plasma

$$\rho_{ext} \approx \rho_{tot} - \rho_{pol}$$

and, from (B.1) and (B.2), we have

$$\epsilon_o k^2 \kappa \phi = \epsilon_o k^2 \phi - e(n_{1i} - n_{1e})$$

Equivalently, we can treat each plasma layer as a dielectric medium with dielectric constant κ for a low frequency flute analysis. Then, using the quasi-neutrality condition in each region and the uniqueness of the charge density at the boundary since there is no free charges, the boundary condition for Eq. (25) becomes,

$$\hat{n} \cdot \{\kappa \vec{E}\} = 0$$

where, $\hat{n}$ is a unit normal vector to the boundary, and $\{\kappa \vec{E}\}$ denotes the increment in $\kappa \vec{E}$ across the boundary.

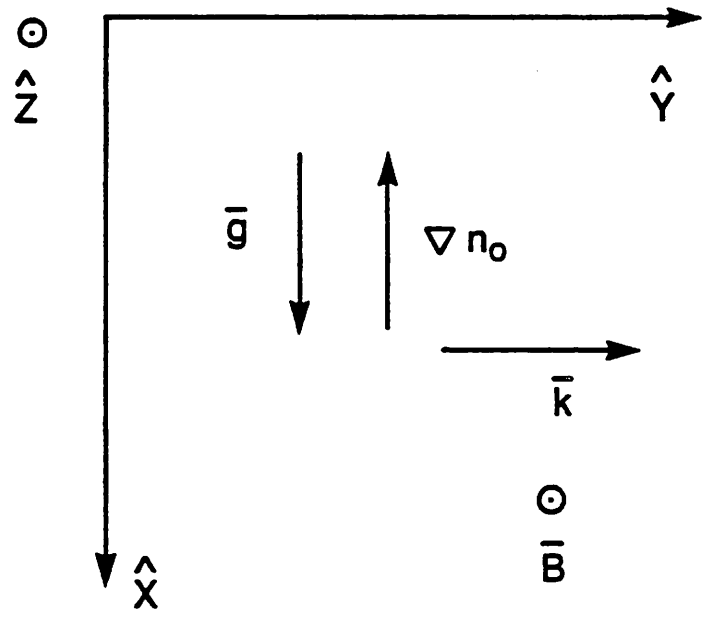

Figure 1. Coordinate system for MHD stability.

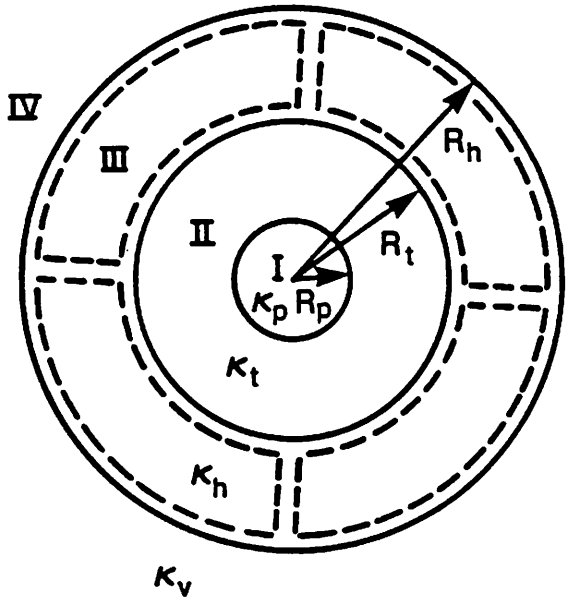

Figure 2. Three layer model for the mirror confined plasma.

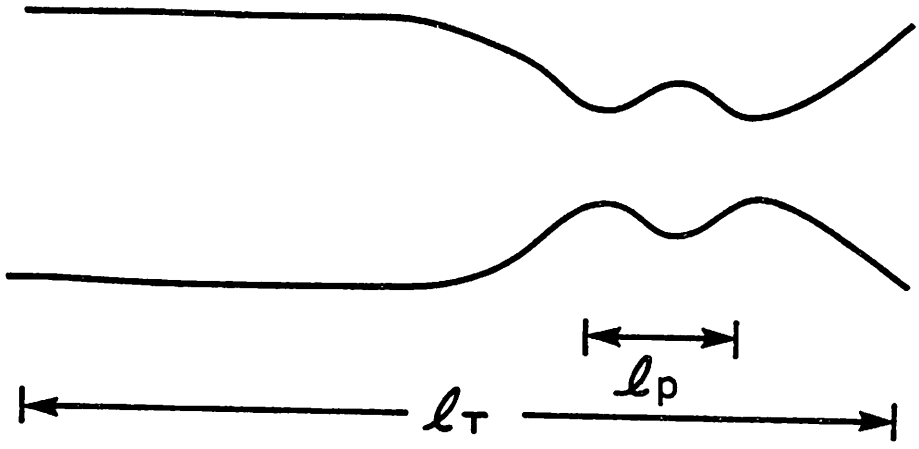

Figure 3. A typical tandem mirror geometry.

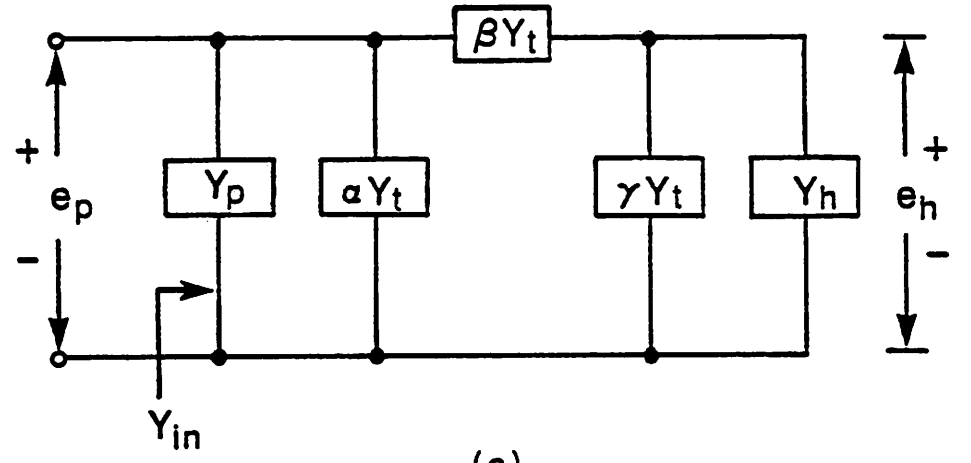

(a)

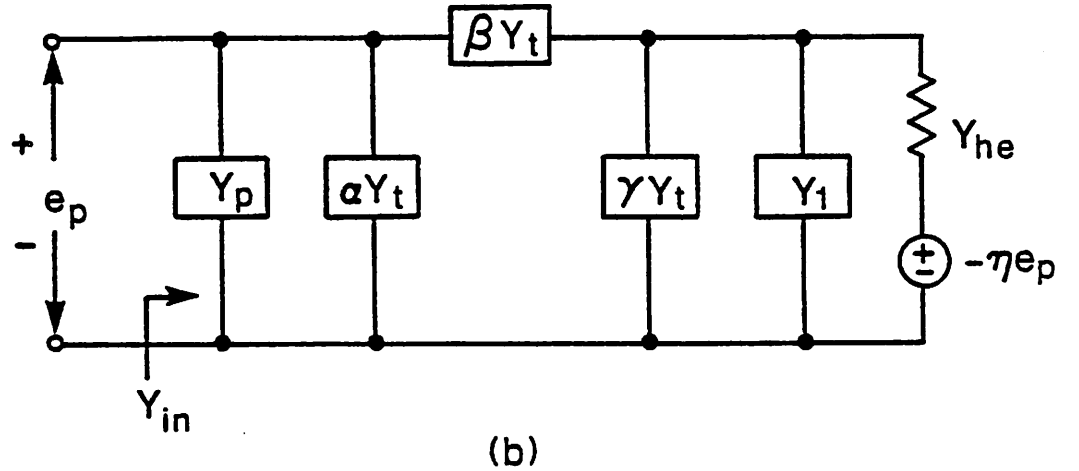

(b)

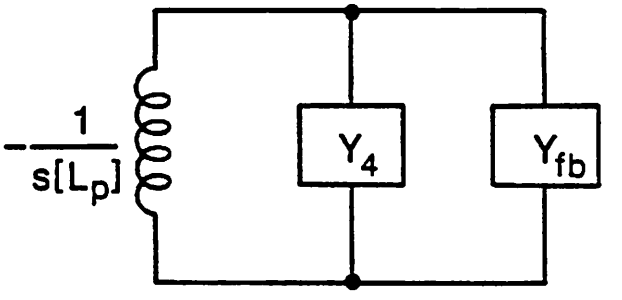

(c)

Figure 4. Circuit representations. (a) three layer model without feedback. (b) three layer model with feedback. (c) equivalent representation of (a), with the negative inductance L_p separated from the rest of the circuit.

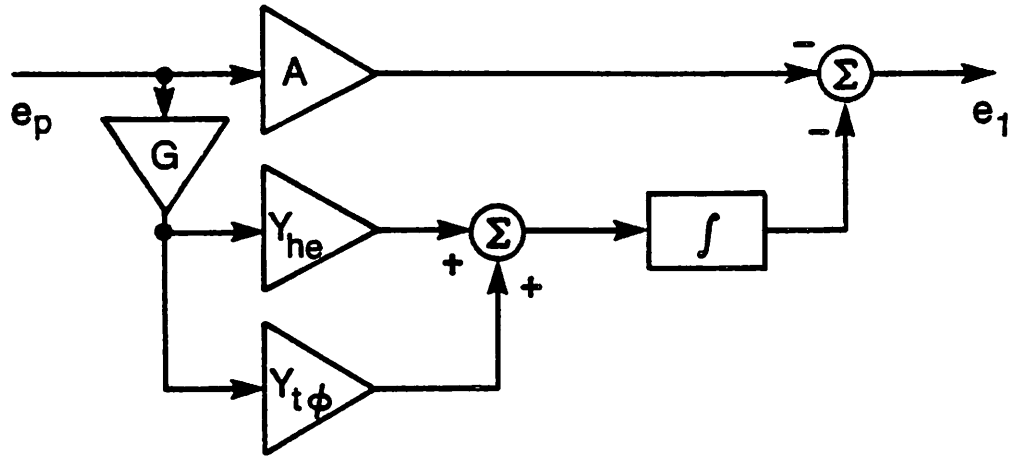

(a)

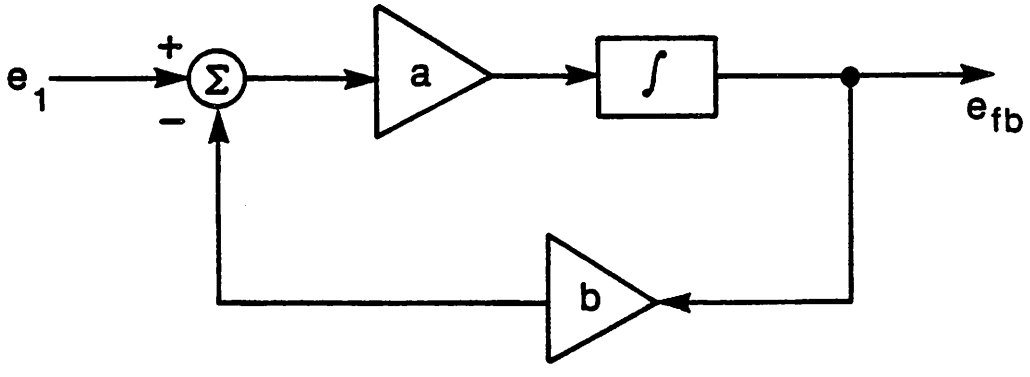

$$a = (\beta |L_p| Y_{he} C_{to})^{-1}$$

$$b = \beta |L_p| Y_{he} Y_{t\phi}$$

(b)

Figure 5. Schematic realizations of (a) $H_1(s)$, and (b) $H_2(s)$.

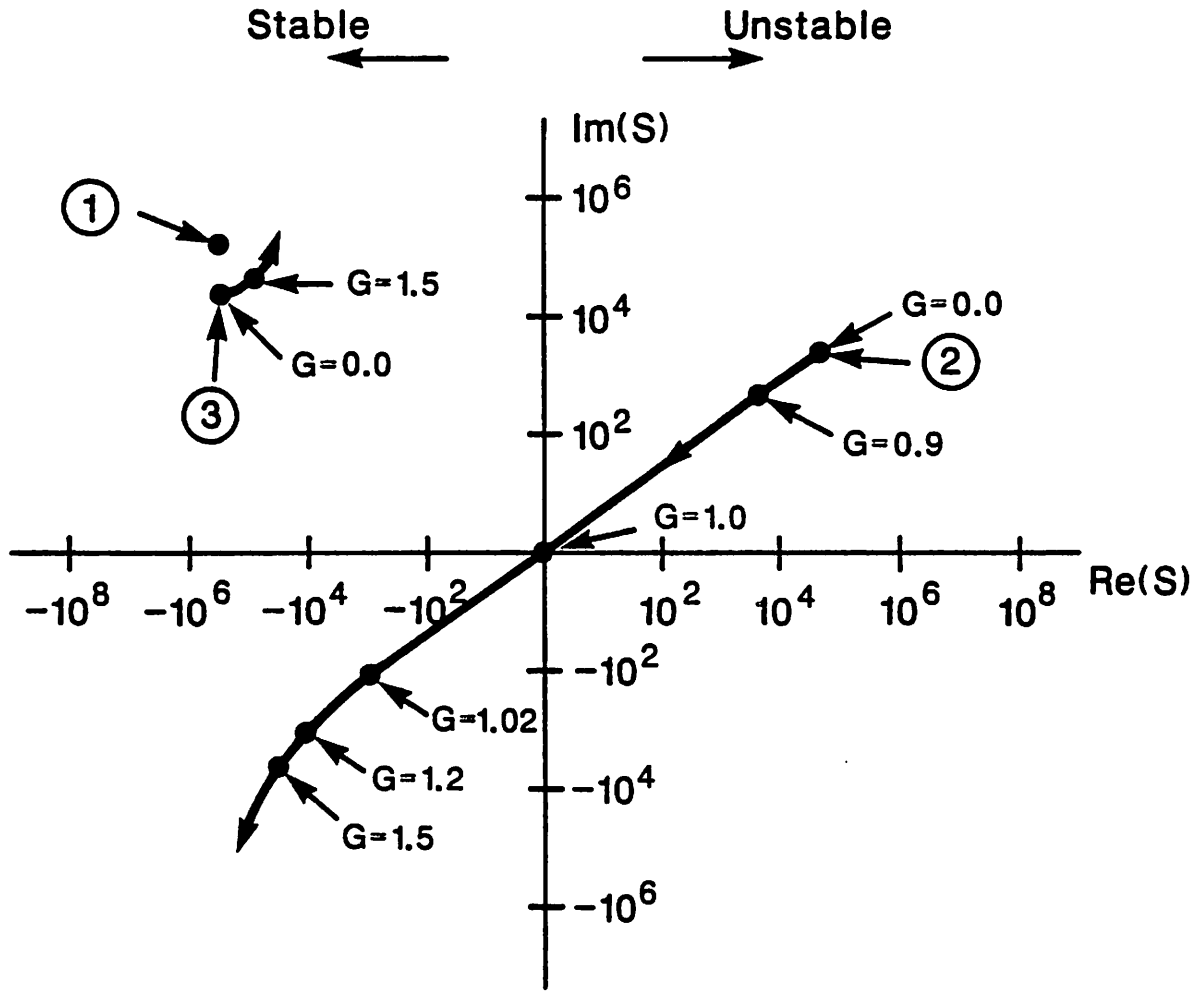

Figure 6. Root loci of the dispersion relation (49) for the MMX.

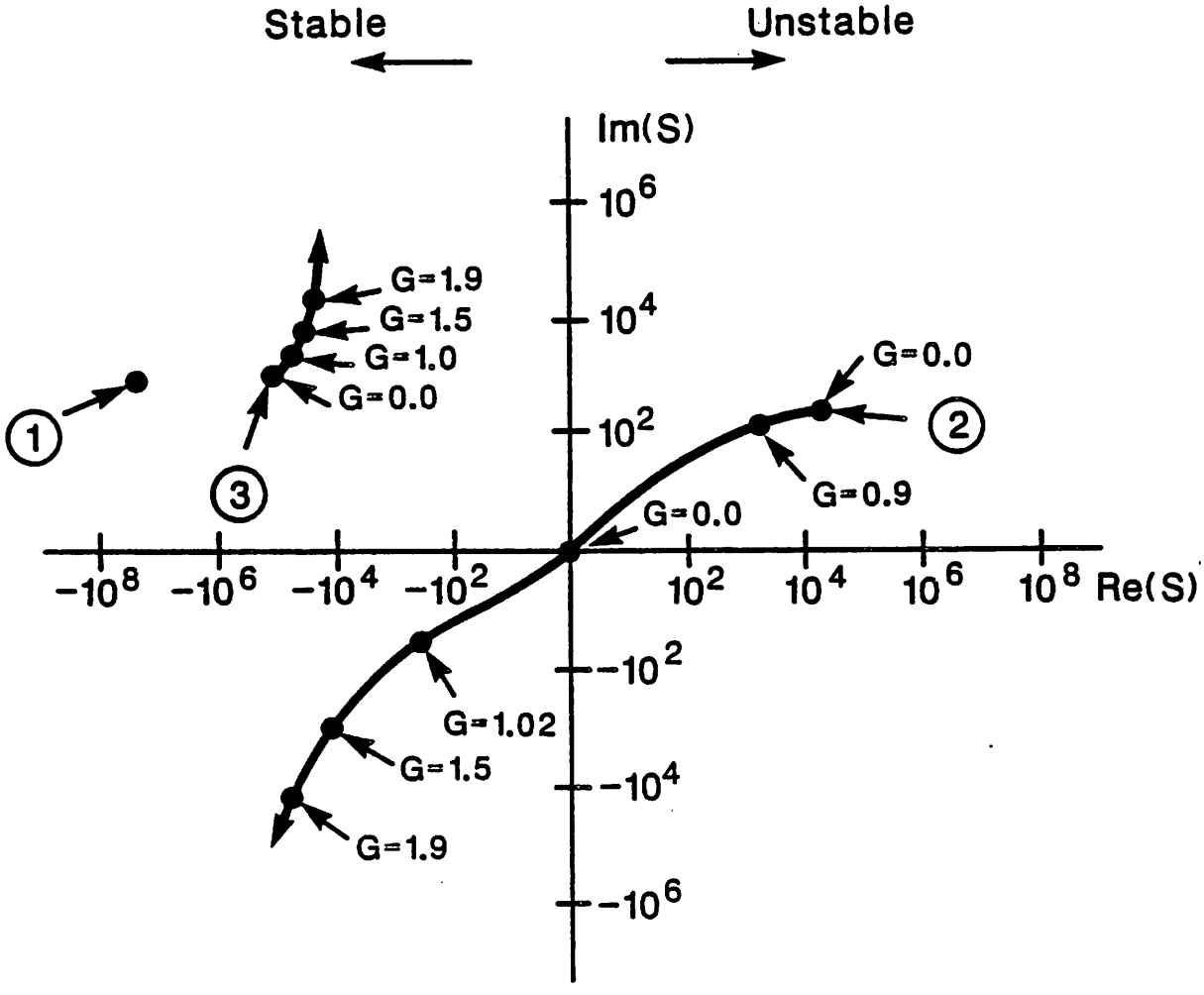

Figure 7. Root loci of the dispersion relation (49) for the TMX-U.

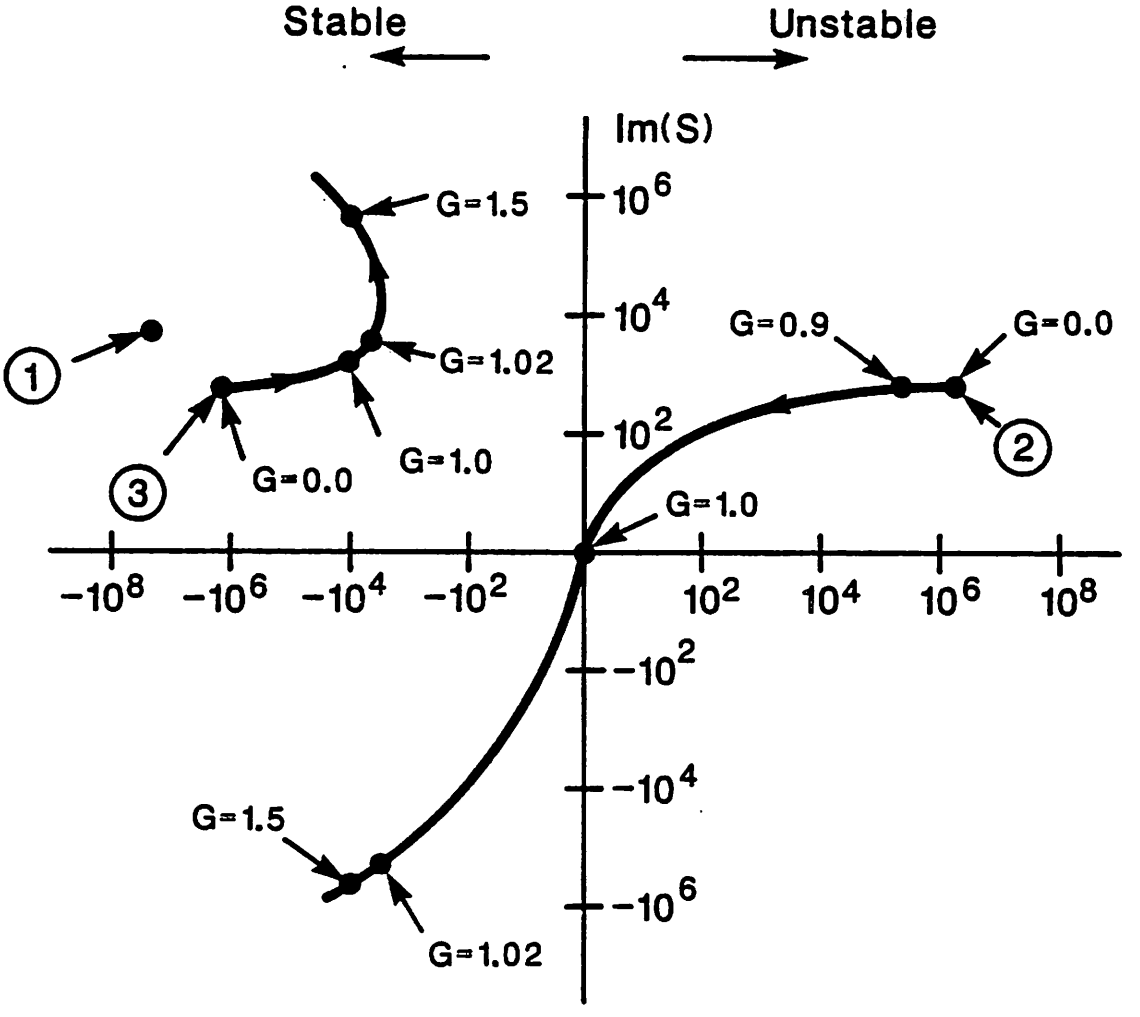

Figure 8. Root loci of the dispersion relation (49) for the MFTF-B.

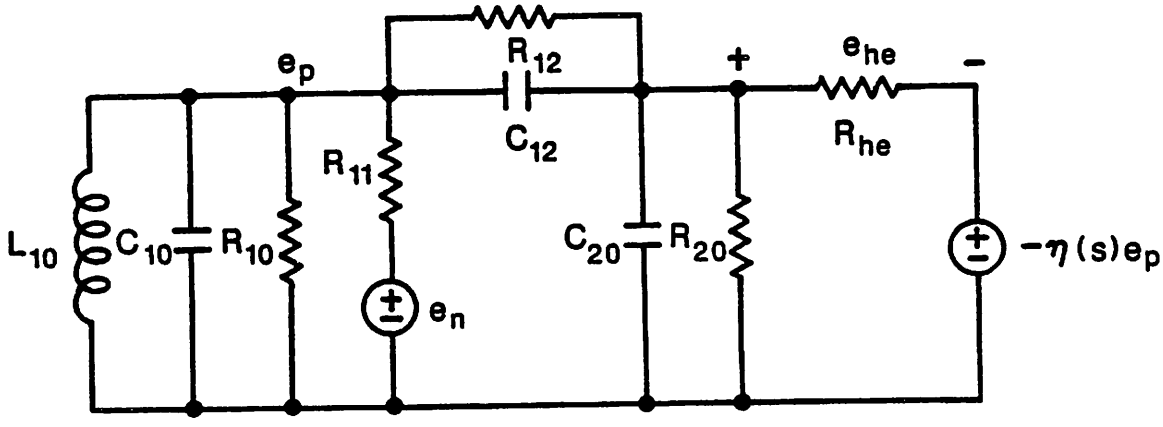

Figure 9. Simulation circuit for Fig. 5b. A noise source voltage e_n is included to represent the plasma fluctuations.

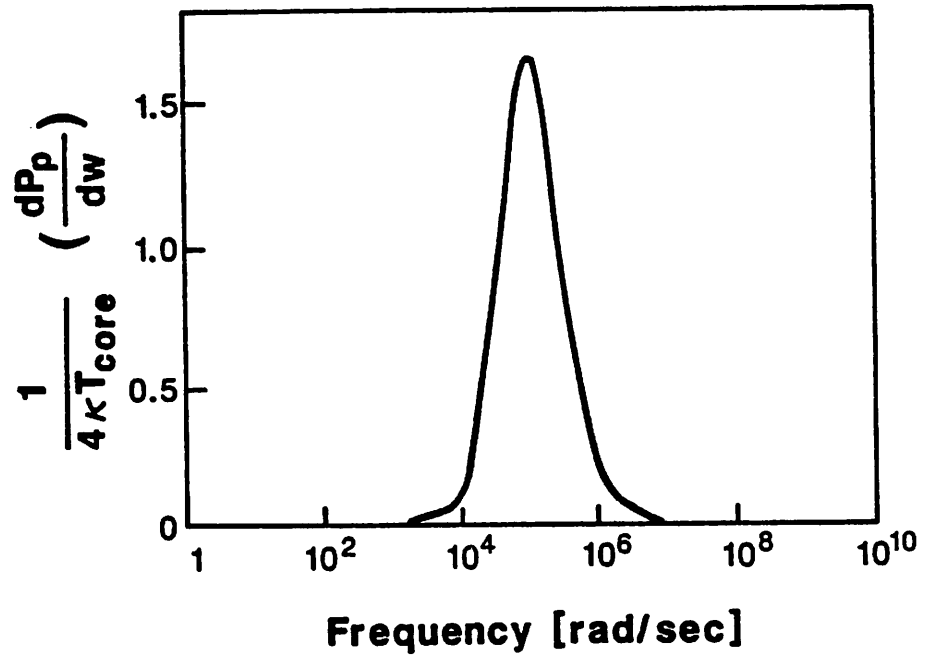

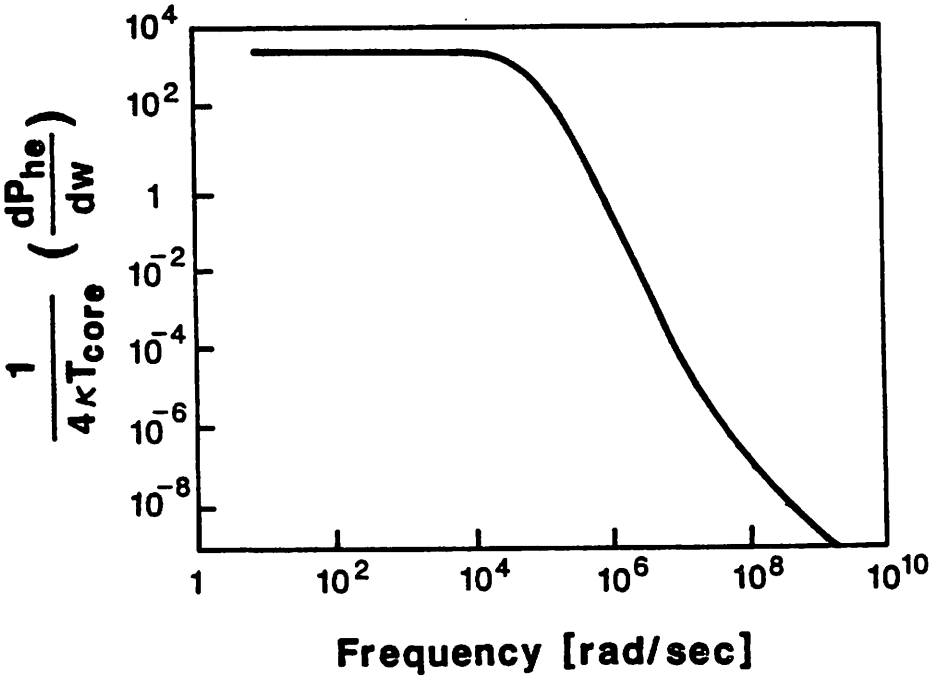

Figure 10. Normalized thermal power spectrum of MMX (a) for the core plasma, and (b) for the sheath.

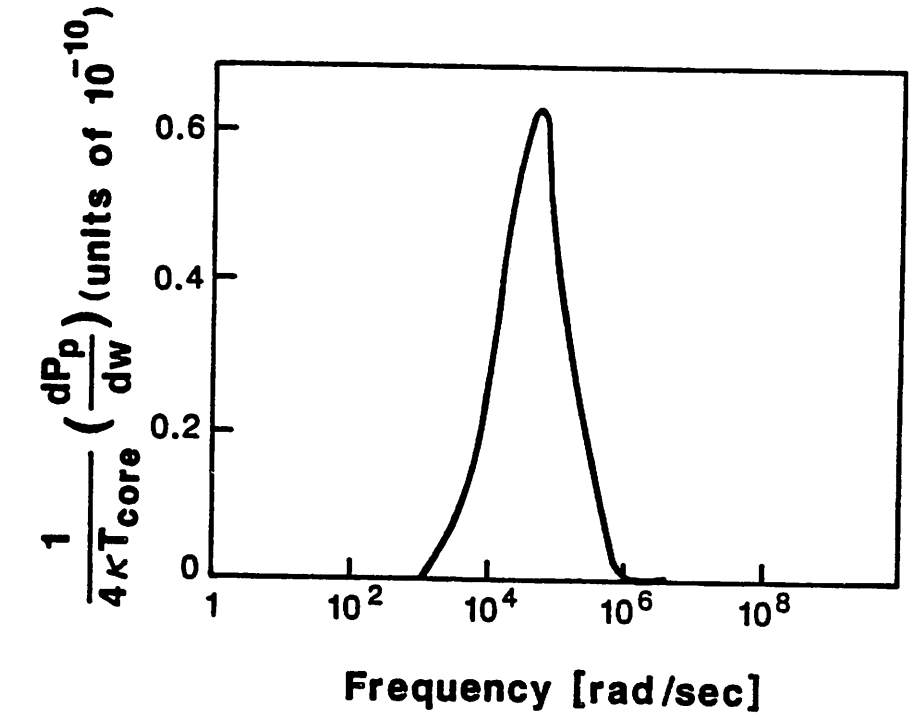

(a)

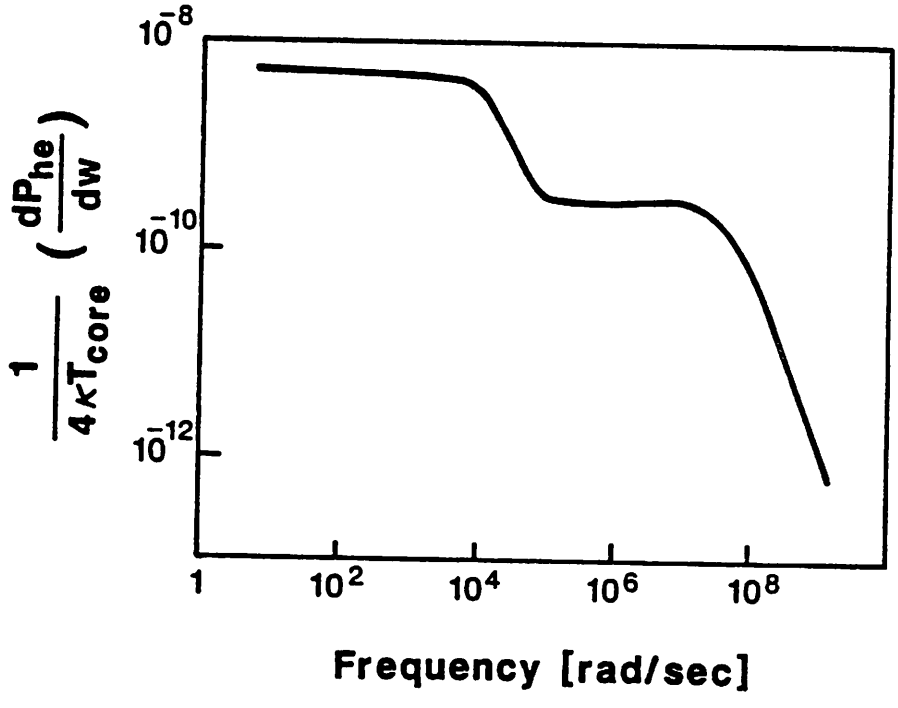

(b)

Figure 11. Normalized thermal power spectrum of TMX-U (a) for the core plasma, and (b) for the sheath.

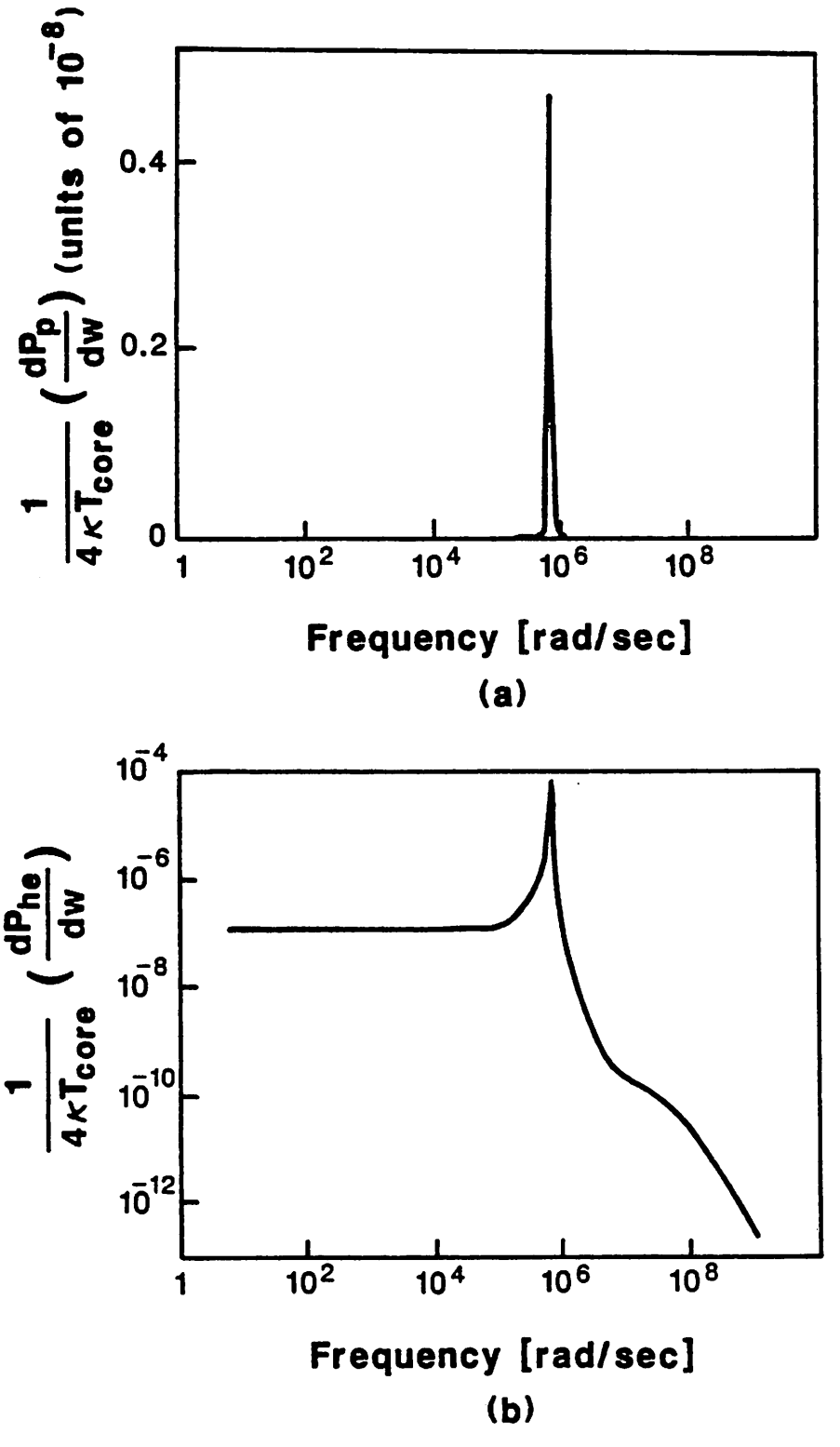

Figure 12. Normalized thermal power spectrum of MFTF-B (a) for the core plasma, and (b) for the sheath.

Table 1. Typical parameters for TMX-U, MFTF-B, and MMX.

parameter	TMX - U	MFTF - B	MMX
$l_B\ [m]$	1	1	0.36
$l_p\ [m]$	3	5	3.75
$l_T\ [m]$	7	12.8	3.75
$R_p\ [cm]$	20	30	2
$R_T\ [cm]$	25	45	3
$R_h\ [cm]$	30	60	4
$n_p\ [m^{-3}]$	10^{18}	10^{20}	10^{19}
n_t/n_p	1	0.1	0.66
n_h/n_p	1	0.1	0.11
$T_p\ [eV]$	100	10^4	10
$T_t\ [eV]$	15	50	10
$T_h\ [eV]$	15	50	10
$B\ [Tesla]$	1	1	0.13

Table 2. Equivalent circuit elements for TMX-U, MFTF-B, and MMX.

	TMX - U	MFTF - B	MMX
$C_{po}\ [F]$	3.86×10^{-8}	6.7×10^{-6}	1.67×10^{-5}
$C_{to}\ [F]$	2.07×10^{-8}	8.4×10^{-7}	9.62×10^{-6}
$C_{ho}\ [F]$	2.53×10^{-8}	1.18×10^{-6}	2.24×10^{-6}
$L_p\ [H]$	-1.65×10^{-3}	-1.00×10^{-7}	-2.89×10^{-6}
$Y_{Rp}\ [mho]$	3.39×10^{-5}	6.3×10^{-4}	3.4
$Y_{Rt}\ [mho]$	2.92×10^{-3}	5.2×10^{-2}	4.44
$Y_{Rh}\ [mho]$	3.51×10^{-3}	6.8×10^{-4}	0.16
$Y_{he}\ [mho]$	8.74	274	0.3
$\omega_I^*\ [rad/sec]$	0	0	0
$\omega_{II}^*\ [rad/sec]$	2.6×10^3	1.0×10^4	2.0×10^5
$\omega_{III}^*\ [rad/sec]$	0	0	0
α	-7.33	-2.7	-2.7
β	15.43	4.8	4.8
γ	15.45	8.2	8.2